A High Resolution Radar-Acoustic Sensor for Detection of Close-in Air Turbulence

Graham Brooker (*Author*), Javier Martinez
ACFR/AMME, University of Sydney
Sydney, Australia
gbrooker@acfr.usyd.edu.au

Duncan Robertson
Physics and Astronomy, St Andrews University
St Andrews, Scotland
dar@st-andrews.ac.uk

***Abstract* - This paper presents a novel 2D imaging sensor for the identification of regions air turbulence in front of a UAV. It comprises a swash-plate mirror scanned Radar Acoustic Sounding System (scaRASS) to produce high resolution "images" of the air in front of the UAV. The 40 kHz/ 17 GHz narrow beam RASS produces images based on Bragg enhanced Doppler radar reflections from the acoustic pulse as it travels. The technique is suited to imaging still air, or air moving in a laminar fashion but returns will be disrupted by air turbulence, so the 3D image generated will identify clear regions in front of the UAV.**

Keywords—radio acoustic sounding; RASS; imaging; ultrasound

I. Introduction

Reflection of electromagnetic radiation from abrupt changes in atmospheric characteristics is now a well known effect. From the beginnings of radar use in WWII it was one of the phenomena that produced artefacts called "angels" [1]. However, it was not until the late 1950s that the changes in refractive index in air induced by acoustic signals were first identified [2]. Over the next 50 years the phenomenon has been used to produce progressively more sophisticated radio-acoustic sounding systems (RASS) to examine air temperature, wind profiles and turbulence in the lower troposphere [3-5].

By the early 1990s, the technique was being applied to indoor problems [6-9] and the application was being widened to other fields, such as IFF [9] and the detection of wake vortices [10, 11].

This combination of RASS with a conventional swash-plate scanner based on our mining radars [12] produces a novel imaging sensor that will be capable of generating images of still or laminar-flow air in three dimensions, and thus, identifying regions of air turbulence.

II. Operational Principles

As an acoustic wave propagates through the air, the density of the medium in one region periodically increases and decreases in a manner which makes these peaks and troughs appear to travel in the direction of propagation. These changes in density result in subtle differences in the refractive index, n, between peak and the trough. When an electromagnetic wave passes through the air, in which these acoustically induced changes in density occur, a small fraction of the signal will be reflected at each of the transitions.

A. Bragg Matching

Bragg matching occurs where the electromagnetic wavelength is equal to twice the acoustic one which results in small reflected components adding in phase to form a larger return as seen in Fig. 1 for a 40 kHz acoustic signal.

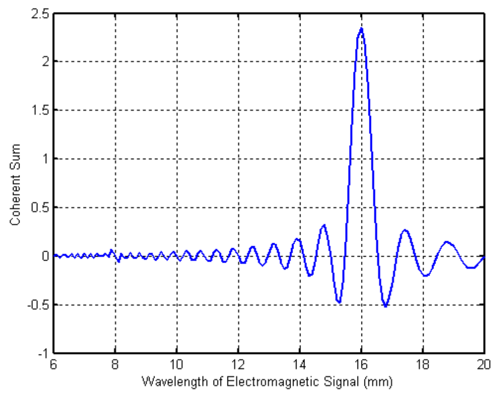

Fig. 1. Coherent sum of the reflected signals shows the Bragg condition

The amplitude of the coherent sum increases linearly with the number of acoustic cycles, *N*. As the received echo power is proportional to the square of the amplitude, it will be proportional to N^2. In addition the width of the Bragg region decreases proportionally. In the RASS case, the Bragg reflector is not static, but a pulse of sound travelling out from the transducer at a velocity $v_a \approx 340$m/s. It is easy to show that if the acoustic and electromagnetic sensors are collocated, a Doppler shift equal to the acoustic frequency, f_a occurs.

$$f_d = \frac{v_a}{\lambda_a} = f_a . \qquad (1)$$

B. Effect of the UAV Speed

The change in acoustic wavelength $\Delta\lambda_a$ (m) for a radial velocity v_r (m/s), will be

$$\Delta\lambda_a = \frac{v_r}{f_a} \qquad (2)$$

This will have the effect shifting the wavelength ratio, and the coherent sum shown in Fig.1 will shift away from the peak. To account for this, it will be necessary to adjust the acoustic or the electromagnetic frequency slightly.

C. Focus Effect

One feature of collocating the acoustic and radar sensors is the focus effect shown in Fig. 2. In this geometry, both the wave-fronts expand with the same radius of curvature and so coherence is maintained over the full area of the expanding pulse [9].

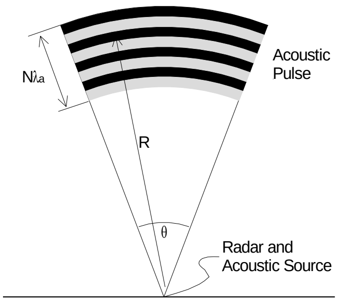

Fig. 2. RASS geometry illustrating the focus effect of collocated sensors

According to Clifford [13], the received power, P_r (W) returned from reflection off an acoustic pulse, if the RF beamwidth is wider than the acoustic beamwidth, can be approximated by

$$P_r = 4.6\times10^{-17}\,\frac{N^2 P_a P_t}{R^2}\left\{\frac{\sin\left[\left(k_a-2k_e\right)\frac{N\lambda_a}{2}\right]}{\left(k_a-2k_e\right)\frac{N\lambda_a}{2}}\right\}\frac{g_e^2}{g_a} \quad (3)$$

where P_t – transmitted RF power (W)

P_a – transmitted acoustic power (W)

g_a – acoustic antenna gain

N – number of acoustic pulses

R – Range (m)

λ_a – acoustic wavelength (m)

$k_a = 2\pi/\lambda_a$

$k_e = 2\pi/\lambda_e$

This is only true if the conditions are perfect and there are no atmospheric perturbations. In the event that the radar beamwidth is narrower than the acoustic beamwidth, then g_e^2/g_a. is replaced by g_a.

Marshall [5] provides an almost identical equation but a factor of three larger.

The radar cross section (RCS), σ_a (m^2), of this expanding acoustic pulse can be determined in terms of the acoustic power, P_a, the acoustic antenna beamwidth, θ_a (rad) and the range, R (m). If the radar beam is wider than the acoustic beam [9] then

$$\sigma_a = \frac{1.76\times10^{-15}\times4\pi^5 R^2 N^2 P_a g_a\left(1-\cos\frac{\theta_a}{2}\right)^2}{16\lambda_a^2} \quad (4)$$

With some simplification (4) reduces to

$$\sigma_a = 1.69\times10^{-12} R^2\theta_a^2 N^2 P_a \quad (5)$$

where θ_a (rad) is the acoustic beamwidth.

D. Effect of Turbulence

The effects of turbulence are twofold. Firstly, local changes in the direction of the airflow can distort the propagation of the acoustic pulse to reduce the effectiveness of the Bragg matching. Secondly, more global turbulence can affect the curvature of the pulse to reduce the focus effect for a collocated sensor configuration.

Together these effects will reduce the effective RCS with the result that the tracked pulse will be extinguished over a short distance. The rate at which the reduction in the echo return occurs, will be indicative of the magnitude of the turbulence in that direction.

E. Atmospheric Attenuation

The equation describing the RCS does not consider the attenuation of the acoustic signal, which increases significantly with increasing frequency[14] [15]. At 40 kHz the attenuation varies between 1.1dB/m and 1.4dB/m depending on the relative humidity. The attenuation corresponding to the range of operation should be subtracted from the RCS calculated in (4) to produce the true value.

III. System Configuration

A. Monostatic RASS Radar System

The wavelength of an acoustic system operating at 40kHz is 8.5mm. The radar system must operate at a wavelength of 17mm to satisfy the Bragg condition, which equates to a frequency of 17.65GHz. A conventional Doppler radar system with reflected power canceller (RPC) has been constructed from discrete components as shown in Fig. 3.

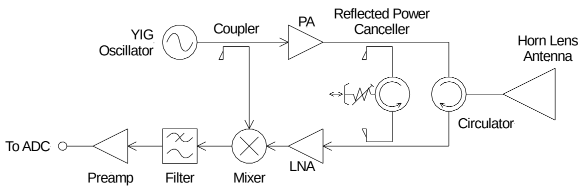

Fig. 3. Schematic diagram of the Doppler radar and reflected power canceller

The RASS performance has been determined in simulation. The RCS defined in (4) and modified by the atmospheric attenuation is plotted in Fig. 4. For an acoustic power of 1 W, it can be seen that the RCS reaches a maximum at a range of 6.5m before falling off as the atmospheric attenuation begins to dominate over the R^2 term.

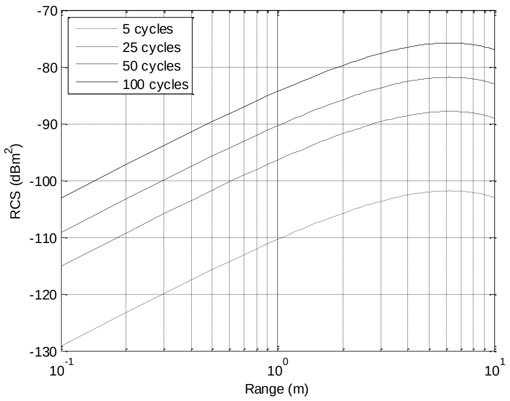

Fig. 4. Radar cross section of acoustic pulse with the number of cycles, N, in a pulse as a parameter

The Doppler radar model assumes that the received signal to noise ratio is limited by thermal noise because the RPC cancels the phase noise leakage effects. The system performance shown in Fig. 5 is determined for the following parameters:

- Operational frequency 17.65GHz
- RF Transmit power 24dBm
- Antenna gain 25dB
- Receive filter bandwidth 3kHz
- System noise figure 5dB
- 100 pulses integrated

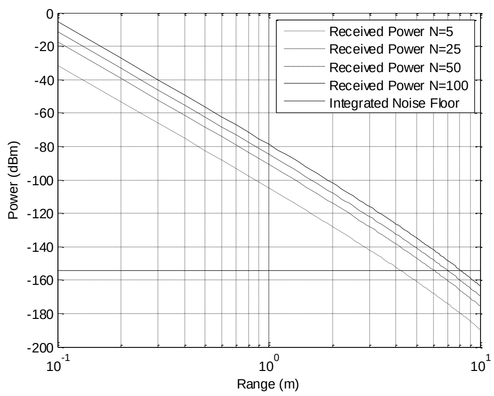

Fig. 5. Received signal and noise levels with the number of cycles, N, in a pulse as a parameter

Because the acquisition of the Doppler signal can be synchronized with the generation of an acoustic pulse, it is possible to integrate a large number of measurements to improve the SNR. For example, for a 10 m maximum range, each measurement takes 30ms, so the coherent integration of 25 returns, would only require 750 ms to perform.

The number of cycles in a pulse should be selected depending on the spatial resolution required and the available SNR. For an acoustic wavelength of 8.5mm, and N = 60, the pulse spans a range of 510 mm which defines the spatial resolution for the received Doppler measurement. As the range is decreased, the available SNR increases and fewer cycles can be used with a resulting improvement in the spatial resolution.

B. *Data Acquisition and Processing*

The controller consists of a laptop and the Data Translation DT9836 USB based IO module. This module includes a 16bit ADC sampling at up to 225 kS/s to acquire the Doppler signal and 16-bit DACs running at 500 kS/s to generate the acoustic pulses. A one channel of stereo hifi amplifier was used to drive the acoustic array.

Software was developed using DT Measure Foundry which allows the synchronous generation of acoustic pulses and the acquisition of the radar outputs as well as some real-time processing. Once sufficient measurements have been sampled and coherently integrated, the Doppler frequency can be extracted from the composite using a moving-FFT based spectrogram [10].

The amplitude of received Doppler signal is determined as a function of time, and it is compared to the still air profile. An unexpected knee where the profile diverges from theory indicates that the acoustic signal is being scattered. The sharpness of the knee is a function of the length of the acoustic pulse, the spectral estimation method and the amount of overlap selected between successive estimates.

IV. System Measurements

A. *Reflected Power Canceller Performance*

Waveguide to SMA adapters were attached to the two waveguide ports of the Doppler radar, shown in Fig. 6, and these coupled to the two terminals of a claibrated 8510 Network Analyzer. The S11 and S21 measurements were conducted for a number of configurations.

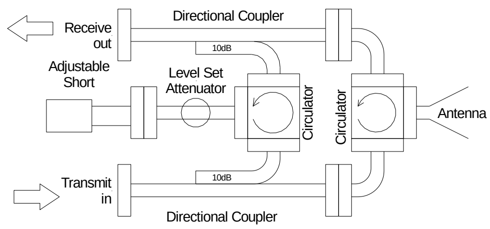

Fig. 6. Block diagram of the waveguide components of the Doppler radar portion of the RASS

B. *Shorted Antenna Port*

This test was conducted to determine how well the components were matched and to ascertain the magnitude of the waveguide and component losses compared to specifications. The level set attenuator component of the RPC is set to maximum attenuation to minimise its affect in this test.

TABLE I. Specified Losses Through the Waveguide Sections

Component	Loss (dB)
Circulator JQL JCWR62-40	0.3×2
Coupler Penn Eng 5038-111A-10	0.46+0.003×2
W/G bends 2038-11A	0.003×2
W/G to Coax Penn Eng 1438 1AM5	0.055×2
Coax bends (measured)	0.22×2
Total	1.62dB

Note that the 0.46dB loss through each coupler corresponds to the proportion of the power tapped off by a 10dB coupler, $10\log_{10}(1-10^{-10/10}) = 0.458$dB

The measured return and transmission losses over a 1 GHz bandwidth from 17 to 18 GHz are shown in Fig. 7.

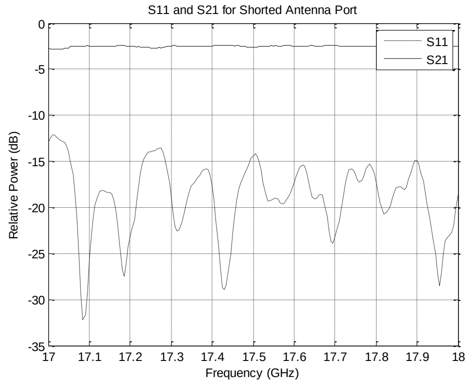

Fig. 7. Measured return (S11) and transmission (S21) losses for the waveguide sections of the RASS with minimal contribution from the RPC

It can be seen that the overall component matching is reasonable with a typical return loss of -15dB. However, the transmission losses of 2.5dB across the band are nearly 1dB higher than the 1.62 dB calculated in Table I. No attempt was made to identify the culprits.

C. Antenna Port with Matched Load

This test was conducted to determine how well the RPC could perform under ideal conditions. As can be seen from Fig. 8, return loss remained below -15 dB, while the transmission loss could be adjusted to produce extremely deep narrow band nulls of -60 dB and more. This confirms that the RPC functions as specified.

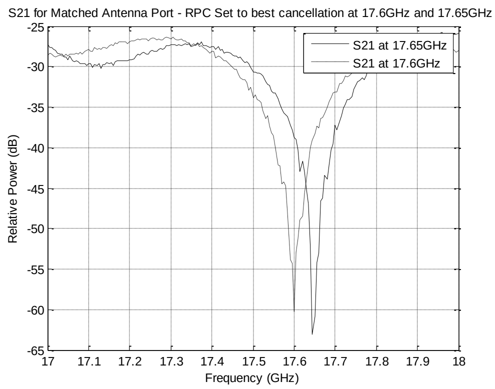

Fig. 8. Measured transmission losses for the waveguide sections of the RASS with the RPC adjusted for maximum cancellation at 17.6 and 17.65 GHz

D. Antenna Port with a Standard Gain Horn

The measured results shown in Fig. 9 confirm that reflected power cancellation is also dependent on close in clutter returns, but that good cancelation is possible under normal, non-specular conditions under which the RASS will operate.

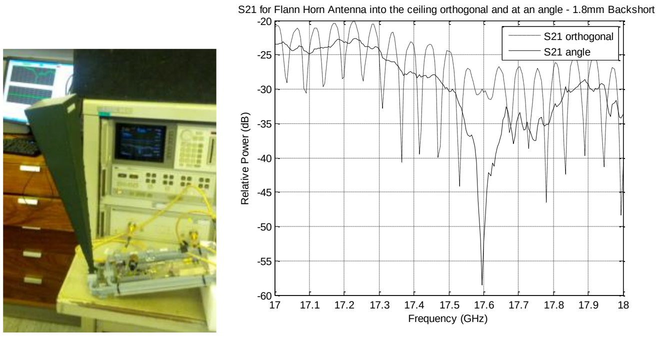

Fig. 9. Photograph of the RASS with the standard gain horn antenna and return loss tuned to 17.6 GHz with the beam perpendicular to the ceiling and at an angle

E. Radar Receiver Requirements

Fig. 5 predicts that the received Doppler echo power from an acoustic pulse will be something between -135 and -155dBm at a range of 4m. This signal needs to be amplified by at least 100 dB to reach mV levels suitable for the ADC board. This gain is achieved by a pair of cascaded RF amplifiers providing 53 dB of gain and an audio amplifier and filter with a further 57 dB of gain at 40 kHz as shown in Fig. 10.

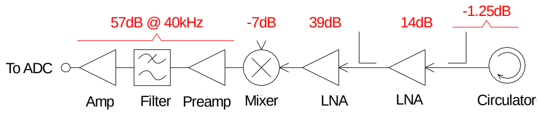

Fig. 10. Block diagram showing the components of the receiver chain

The audio amplifier gain characteristics were configured with sufficient bandwidth to accommodate variations in the Doppler frequency of the received signal due to either changes in temperature or the speed of the UAV.

V. SYSTEM HARDWARE

A RASS was built using a polarised wire reflector in a space frame structure documented by Weiβ [8]. This configuration is shown in Fig. 11. To minimize microphonics, which had plagued earlier configurations of the system, the acoustic array was hung from rubber bands (not visible).

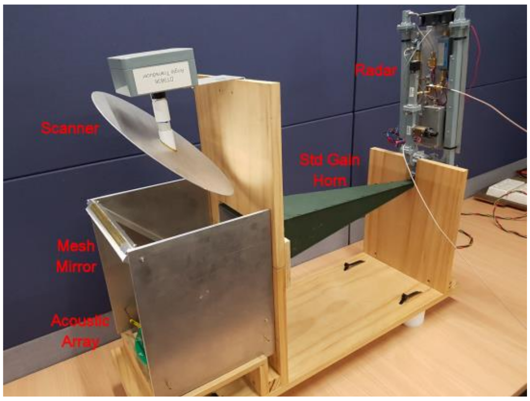

Fig. 11. Photograph of the scanning RASS sensor with the various components labelled

A. System Calibration

To measure the system performance, it is convenient to use a Doppler reflector with a known RCS. Conventional moving targets are not suitable as the receiver is tuned to provide maximum sensitivity at around 40 kHz, which corresponds to a velocity of 340 m/s. In addition, the expected RCS is incredibly small, as can be seen in Fig. 5.

To achieve this, a small Doppler target was developed using a 40 kHz piezo transducer and a small ball bearing. Sinusoidal excitation voltages of between 1V and 10V produced variations in the measured RCS from -140.5 dBsqm to -120.5 dBsqm [16].

VI. Ranging

The system was first operated in vertical-pointing mode (without the scanner component) to determine its performance under different conditions.

To confirm that the acoustic array was well isolated from the Doppler radar, system was first operated with the transmit aperture blocked. It can be seen from Fig. 12 that apart from the acoustic bang pulse every 20 ms, the signal level is constant. This is verified in Fig. 13 which shows the spectrogram is empty at 40 kHz apart from the bang pulse period.

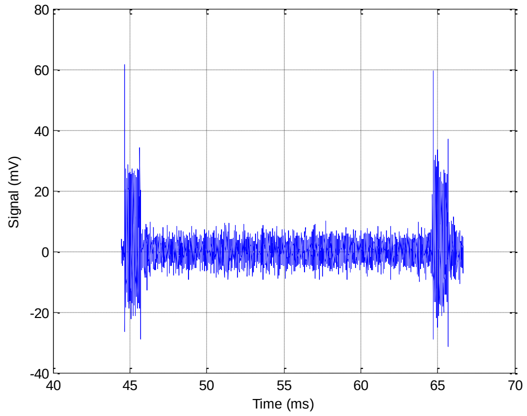

Fig. 12. Time domain signal received by the Doppler radar with the transmit aperture blocked

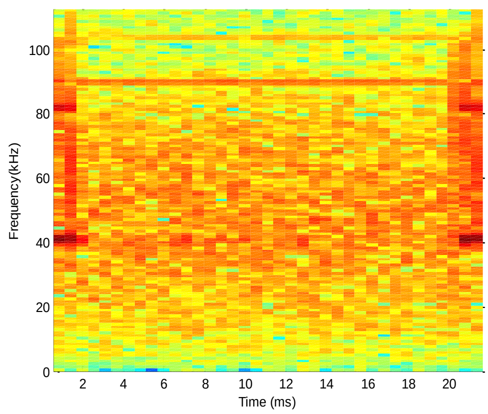

Fig. 13. Spectrogram of the Doppler signal with the transmit aperture blocked

The second test conducted in still air outdoors shows an exponentially decaying signal amplitude as a function of time with some modulation (Fig. 14). The spectrogram shown in Fig.15, confirms that echoes is received right up to the start of the next pulse 20 ms later. This corresponds to a range of 6.8 m at a nominal speed of sound of 340 m/s.

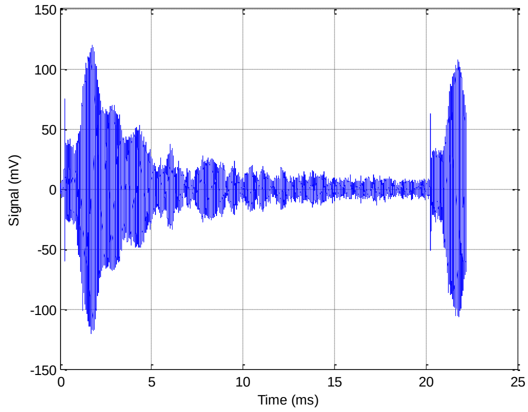

Fig. 14. Time domain signal received by the Doppler radar for operation outdoors

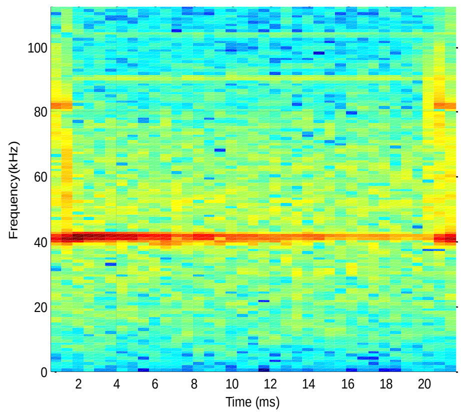

Fig. 15. Spectrogram of the Doppler signal for operation outdoors

The final test, with results shown in Fig. 16 and Fig. 17, shows the results for operation indoors with a roof height of 5m. In this case, the signal attenuates following the normal exponential decay profile, but ends after 15 ms.

Note that the differences in the peak amplitudes of the time domain in Fig. 14 and Fig. 15 are as a result of the changed VSWR, and hence sensitivity, of the system when operated outside where there is very little reflected power, and indoors pointing towards a flat roof.

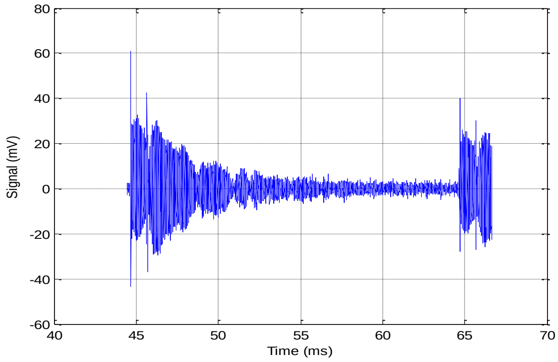

Fig. 16. Time domain signal received by the Doppler radar for operation indoors towards the roof at a range of 5m

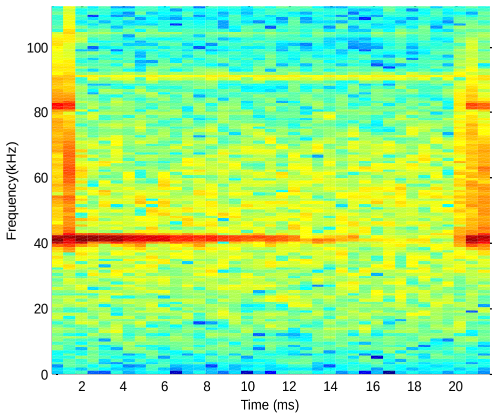

Fig. 17. Spectrogram of the Doppler signal for operation indoors towards the roof at a range of 5m

VII. Conclusions

This paper has discussed the development of a novel RASS comprising an array of one hundred 40 kHz ultrasonic elements collocated with a sensitive Doppler radar. The large acoustic aperture and high frequency result in a narrow beam which allows for the remote measurement of atmospheric turbulence within a small volume in space (0.25m×0.25m×0.25m) at a range of 7m.

Measurements were made to confirm the operation of the sensor in its vertical ranging mode, and it was able to detect acoustic pulses out to beyond 6.8m.

A swash plate scanner, developed for our mining applications, was integrated to direct the beam but could not be tested in time for inclusion in this paper. However, once this is achieved, a sector of space in front of the system will be scanned to generate a 3D map of regions of air turbulence.

Once this proof of concept has been established, the next phase will be to harden and integrate such a system onto a fixed-wing UAV for airborne tests.

References

[1] M. Skolnik, *Introduction to Radar Systems*, 2nd ed.: McGraw-Hill Kogakusha, 1980.

[2] A. Tonning, "Scattering of Electromagnetic Waves by an Acoustic Disturbance in the Atmosphere," *Applied Science Res.*, vol. B6, pp. 401-421, 1957.

[3] N. Bhatnagar and A. Peterson, "Interaction of Electromagnetic and Acoustic Waves in a Stochastic Atmosphere," *IEEE Trans. on Antennas and Propagation*, vol. AP-27, pp. 385-393, May 1979.

[4] M. Frankel, N. Chang, and M. Sanders Jr, "A High-Frequency Radio Acoustic Sounder for Remote Measurement of Atmospheric Winds and Temperature," *Bulletin American Meterological Society*, vol. 58, pp. 928-933, September 1977.

[5] J. Marshall, A. Peterson, and A. Barnes Jr, "Combined Radar-Acoustic Sounding System," *Applied Optics*, vol. II, pp. 108-112, January 1972.

[6] M. Daas and R. Knochel, "Microwave-acoustic Measurement System for Remote Temperature Profiling in Closed Environments," in *EUMC*, Helsinki, Finland, 1992, pp. 1225-1230.

[7] M. WeiB and R. Knochel, "A Monostatic Radio-Acoustic Sounding System," *IEEE MTT-S Digest*, vol. THF4-9, pp. 1871-1874, 1999.

[8] M. WeiB and R. Knochel, "A Monostatic Radio-Acoustic Sounding System Used as an Indoor Remote Temperature Profiler," *IEEE Trans. on Instrumentation and Measurement.*, vol. 50, pp. 1043-1047, October 2001 2001.

[9] J. Saffold, F. Williamson, K. Ahuja, L. Stein, and M. Muller, "Radar-acoustic Interaction for IFF Applications," in *IEEE Radar Conference*, Waltham, MA, 1999, pp. 198-202.

[10] J. Hanson and F. Marcotte, "Aircraft Wake Vortex Generation Using Continuous-Wave Radar," *Johns Hopkins Apl. Technical Digest*, vol. 18, pp. 348-357, 1997.

[11] R. Marshall, "Wingtip Generated Wake Vortices as Radar Targets," *IEEE AES Systems Magazine*, pp. 27-30, December 1996.

[12] G. Brooker, M. Bishop, and R. Hennessey, "Evolution of a Suite of Millimetre Wave Radar Systems for Situational Awareness and Automation in Mines," presented at the 2008 Australian Mining technology Conference, Sunshine Coast, QLD, Australia, 2008.

[13] S. Clifford and T. Wang, "The Range Limitation on Radar-Acoustic Sounding Systems (RASS) due to Atmospheric Refractive Turbulence," *IEEE Trans. on Antennas and Propagation*, vol. AP-23, pp. 319-326, May 1977.

[14] L. Kinster and A. Frey, *Fundamentals of Acoustics 2nd Ed*. New York: John Wiley & Sons, 1962.

[15] N. Burnside, "A Function that Returns the Atmospheric Attenuation of Sound," ed: MATLAB Central - http://www.mathworks.com/matlabcentral/fileexchange/loadFile.do?objectId=6000&objectType=FILE, 2004.

[16] G. M. Brooker, "An Adjustable Radar Cross Section Doppler Calibration Target," *Sensors Journal, IEEE*, vol. 15, pp. 476-482, 2015.